UNIVERSITEIT•STELLENBOSCH•UNIVERSITY
jou kennisvennoot • your knowledge partner

Reduction of inverter-induced shaft voltages using electrostatic shielding (repository copy)

Article:

Gerber, S., Wang, R-J, (2019), Reduction of inverter-induced shaft voltages using electrostatic shielding, *Proc. the 27th Southern African Universities Power Engineering Conference*, (SAUPEC), pp. 310-315, 28-30 Jan. 2019, Central University of Technology, Bloemfontein.

ISBN: 978-1-7281-0368-6 / IEEE Catalogue Number: CFP1948U-USB
http://doi.org/10.1109/RoboMech.2019.8704702

Reuse
Unless indicated otherwise, full text items are protected by copyright with all rights reserved. Archived content may only be used for academic research.

2019 SAUPEC/RobMech/PRASA Conference
Bloemfontein, South Africa, January 28-30, 2019

Reduction of Inverter-Induced Shaft Voltages Using Electrostatic Shielding

Stiaan Gerber* and Rong-Jie Wang†
Department of Electrical and Electronic Engineering
Stellenbosch University
Stellenbosch, 7600
South Africa
Email: sgerber@sun.ac.za*, rwang@sun.ac.za†

***Abstract*—The simple three-phase inverter topology that is most widely used in electrical machine drive systems produces a large, high-frequency common-mode voltage. Through capacitive coupling, a fraction of this common-mode voltage typically appears on the machine's shaft relative to ground. The shaft voltage can discharge through the bearings of the machine, causing damage and eventually resulting in premature bearing failure compared with equivalent line-fed machines. As a first step in the investigation of mitigation techniques for this problem, this paper evaluates the use of simple aluminium foil shielding applied to a standard 4-pole induction machine with a rated power of 11 kW for mitigation of bearing currents.**

***Index Terms*—shaft voltage, common-mode voltage, electrostatic shielding, bearing failure**

I. Introduction

Bearing currents in electrical machines are not a new phenomenon. Since the early 1900's, bearing currents have been known to cause bearing failures in line-fed machines [1]. However, improvements in manufacturing accuracy and simple protective measures have solved problems associated with bearing currents in line-fed machines to a large extent.

Interestingly, the problem of bearing currents has returned in a more destructive form with the advent of fast-switching power electronic drives for electrical machines [2]. High-frequency bearing currents that overcome the insulating properties of bearing oil films are alike to the currents generated in *electrostatic discharge machining* (EDM). These currents cause material to be removed between two electrodes. When this type of current flows between bearing races and rolling elements, it leads to a dramatic increase in wear of the bearing and drastically reduces its lifetime.

Of course, this problem is of great significance to industry since it affects the reliability, availability and maintenance costs of electrical drive systems. As such, much research has been done on this problem. The physical mechanisms which lead to damaging bearing currents have been investigated and described in detail [3], [4]. Methods of modeling bearing currents have been presented [5]. Many solutions to the problem have been proposed [6] and products specifically aimed at protecting bearings in electrical drive installations have come to market.

In section II of this paper, inverter-induced bearing currents will be discussed in greater depth. The remainder of the paper deals with a particular type of bearing current commonly found in low voltage induction machines. In section III, a simple model is presented and in section IV, a mitigation strategy using simple aluminium foil shielding is evaluated experimentally. Finally, conclusions are drawn and focus areas for future work are identified.

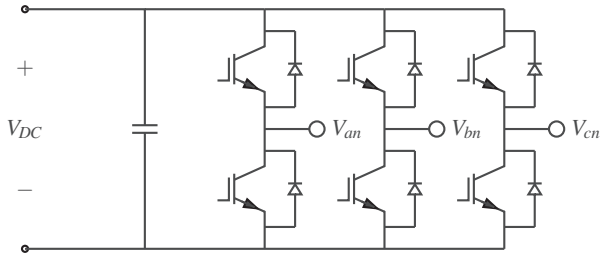

Fig. 1: Standard three-phase inverter topology.

II. Bearing current origins

The driving forces behind bearing currents in inverter-fed machines are more complex than those of classical bearing currents occurring in line-fed machines. At high frequencies, currents can flow across barriers that behave as perfect insulators at lower frequencies. Furthermore, these bearing currents are driven by more than one mechanism. However, the primary source of all inverter-driven bearing currents is the common-mode voltage produced by the inverter. The inverter topology considered here is illustrated in Fig. 1. The common-mode voltage is given by

$$V_{CM} = \frac{V_{an} + V_{bn} + V_{cn}}{3} \tag{1}$$

It is clear that this inverter cannot produce a common-mode voltage equal to zero, since it is not possible to realize a zero common-mode voltage with three voltages, each of which is switched either high or low. A typical common-mode voltage waveform produced by the inverter of Fig. 1 is shown in Fig. 2. The peak-to-peak amplitude is equal to the DC bus voltage and the frequency is equal to the switching frequency.

The common-mode voltage can drive bearing currents in several ways. Firstly, there is capacitive coupling between the winding common-mode voltage and other components of the machine, including the rotor core, shaft, stator core and frame. This capacitive coupling leads to a potential difference across the bearings. The current paths may differ depending on whether the shaft is well grounded, via the driven machinery, or not. These current paths are illustrated

978-1-7281-0369-3/19/$31.00 ©2019 IEEE

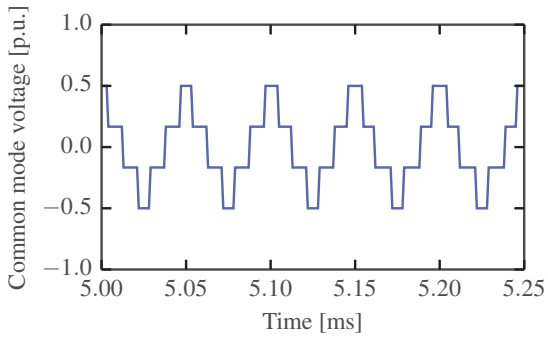

Fig. 2: Typical common-mode voltage produced by a standard three-phase inverter.

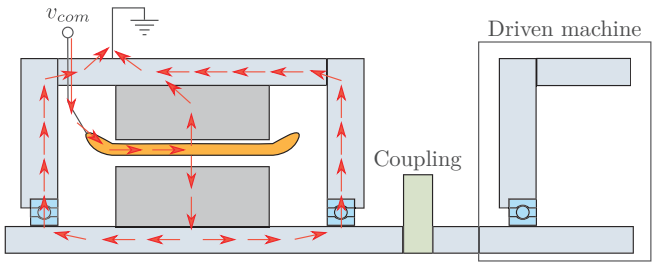

(a) Common mode current leaking to shaft and back across bearings with a well grounded stator frame.

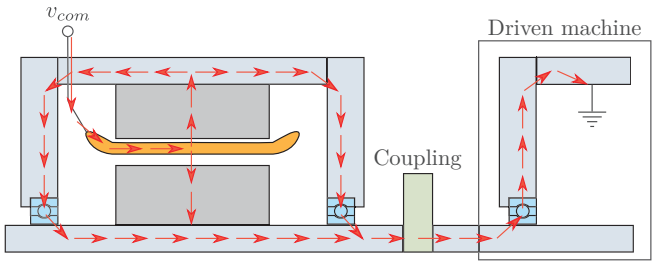

(b) Common mode current leaking to shaft via the air-gap and the bearings when the shaft is well grounded via the driven machine.

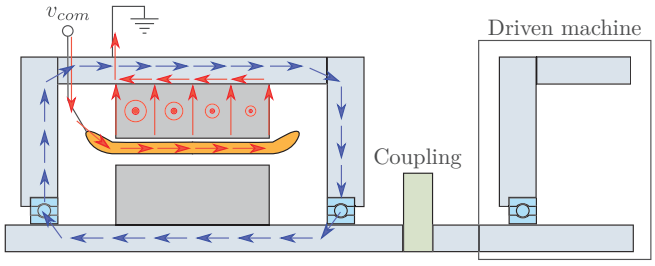

(c) Common mode current (red) driving a time-varying ring-flux in the stator core which induces currents (blue) in the same loop as classical bearing currents.

Fig. 3: Different bearing current paths.

in Figs. 3a and 3b. Secondly, the capacitive coupling of the common-mode voltage results in common-mode currents flowing in the machine. Some of these currents follow a path that generates a ring-flux in the stator core. The high frequency ring flux can drive current in the same loop as that in which classical bearing currents flow. This mechanism is illustrated in Fig. 3c.

In this paper, the focus falls on the type of bearing current illustrated in Fig. 3a, commonly referred to as the

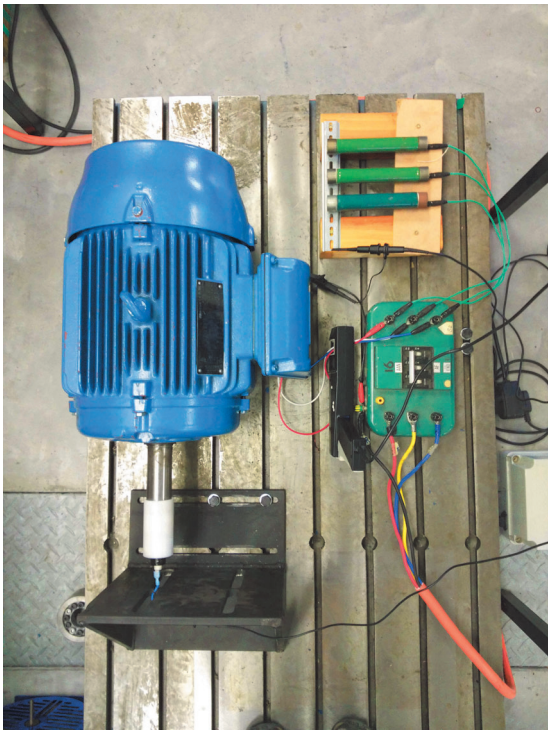

Fig. 4: Overview of test setup.

TABLE I: Motor specifications

Parameter	Value
Rated power	11 kW
Rated voltage (delta)	400 V
Rated current	22 A
Rated speed	1460 rpm
Frame size	160M

electrostatic discharge machining (EDM) current. A simple test bench was setup in order to observe the phenomenon. The test setup is shown in Fig. 4. An inverter drives a standard induction machine at no-load and the common-mode and shaft voltages are measured. Detailed specifications of the machine and the inverter are given in Tables I and II. The machine's windings are delta-connected due to the voltage limit of the inverter. For this reason, the common-mode voltage is measured using an artificial star point, realized by three 50 kΩ resistors. A reliable electrical connection to the rotating shaft is made using a Mercotac connector, shown in Fig. 5. This allows the shaft voltage to be measured accurately.

Typical common-mode and shaft voltage waveforms associated with EDM bearing currents are shown in Fig. 6. These waveforms were observed using the described test setup with the induction machine operating at a fundamental

TABLE II: Inverter specifications

Parameter	Value
Rated power	37 kW
Bus voltage	550 V
Switching frequency	8 kHz

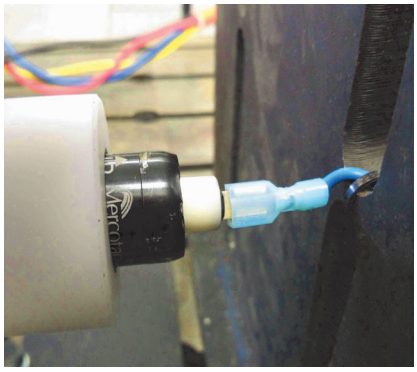

Fig. 5: Stable electrical connection to rotating shaft for shaft voltage measurement.

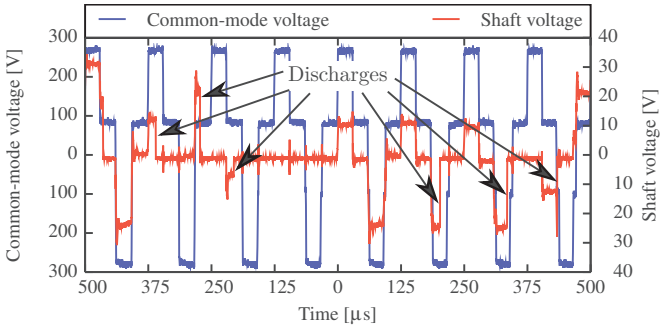

Fig. 6: Observed shaft voltage discharges.

frequency of 30 Hz (approximately 900 rpm). In Fig. 6, it can be seen that the shaft voltage generally mirrors the common-mode voltage, except at a number of instances where the shaft voltage collapses. The collapsing of the shaft voltage is ascribed to discharges across the bearings. These discharges can be verified by measuring the bearing currents. However, bearing current measurements were not available at the time of writing.

III. Modeling of Capacitive Shaft Voltage

The shaft voltage waveform observed in Fig. 6 can be explained with the aid of the simple equivalent circuit diagram shown in Fig. 7 [7]–[9]. In this circuit, C_{wf} represents the capacitance between the stator winding and the frame. This capacitance is generally quite large compared to the other capacitances in the circuit due to the close proximity and large surface area between the winding and the stator core. It is assumed that the stator core is in good electrical contact to the earthed frame. There is also a capacitance between the winding and the rotor, C_{wr}. The magnitude of this capacitance depends on the slot opening, but a large portion is also due to the capacitance between the end-winding and the rotor [10]. The impedance between the rotor and the frame can be represented by a constant capacitance, C_{rf}, in parallel with the impedance across the bearings, which is lumped together in Fig. 7. Modeling the impedance of the bearings is a complex task [11], but in general it can be said that the bearing impedance is capacitive when the shaft voltage mirrors the common-mode voltage and resistive when the insulating film between the rolling elements and the races breaks down.

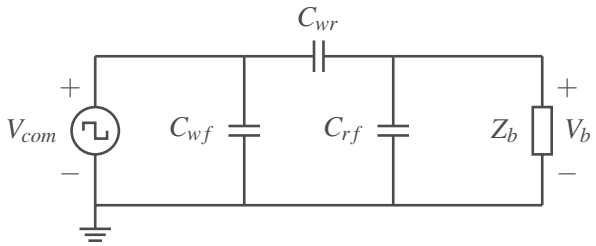

Fig. 7: Simple equivalent circuit model describing capacitive shaft voltage.

Using the circuit of Fig. 7, and assuming that the bearing impedance $Z_b = \frac{1}{\omega C_b}$ where C_b represents the bearing capacitance, an expression for the bearing voltage V_b can be obtained:

$$V_b = V_{CM}\left(\frac{\frac{1}{\omega C_b}\|\frac{1}{\omega C_{rf}}}{\frac{1}{\omega C_b}\|\frac{1}{\omega C_{rf}}+\frac{1}{\omega C_{wr}}}\right)$$
$$V_b = V_{CM}\left(\frac{C_{wr}}{C_{wr}+C_{rf}+C_b}\right) \quad (2)$$

This equation indicates that, in order to minimize the voltage across the bearings, the capacitance between the winding and the rotor C_{wr} should be minimized.

IV. Evaluation of Shielding Configurations

Among the various methods of reducing the problems associated with EDM bearing currents, shielding of the rotor is an attractive option because it has the potential to be an inexpensive yet effective solution [10], [12], [13]. Different methods of implementing the shield have been proposed. As a first step in the evaluation of shielding methods, the induction motor of Table I has been equipped with simple aluminium foil shields in the end-winding region. Referring to Eq. 2, the shields drastically reduce the capacitance between the winding overhang and the rotor. In this way, the shaft voltage is reduced.

The preparation and installation of the aluminium foil shields is illustrated in Fig. 8. The shields were fabricated by glueing household aluminium foil to Nomex paper using double-sided tape. The shields were secured to the end-windings using pieces of string. Electrical connections were routed to the machine's terminal box where they could easily be connected to ground in order to evaluate the effectiveness of the shields or allowed to float to realize and unshielded case.

Measured common-mode and shaft voltage waveforms for the unshielded and shielded configurations are presented in Fig. 9. It can be seen that the shields reduce the magnitude of the shaft voltage by approximately 35 %.

A second, more complete, shielding configuration was also evaluated. In this case, strips of shielding were installed that enclosed the end-winding regions, as well as the entire inner bore of the stator. Each of the strips was then connected to a copper ring which could be earthed to shield the rotor or left floating to represent the unshielded case. The fabrication, installation and connection of these shields are illustrated in Fig. 10. Again, measured common-mode and shaft voltage

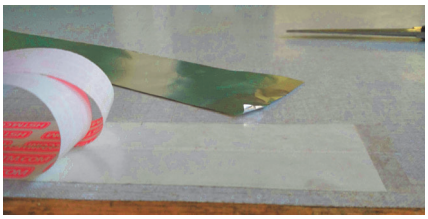

(a) Fabrication of shielding material.

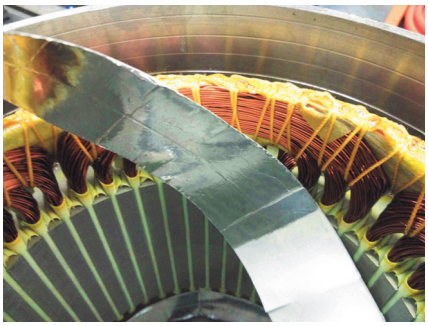

(b) End-winding region to be shielded.

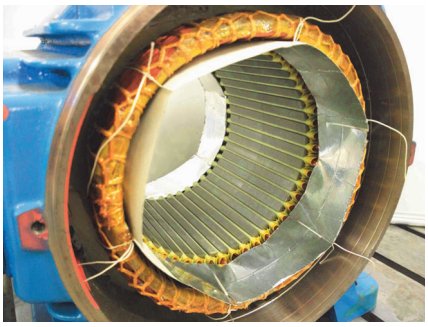

(c) Shield tied to end-windings.

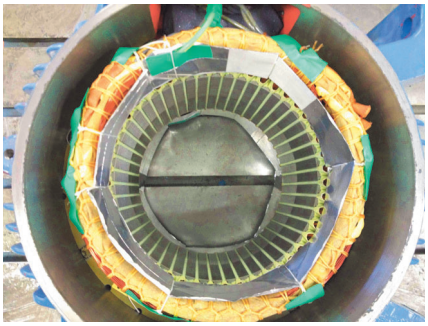

(d) Shield installation completed.

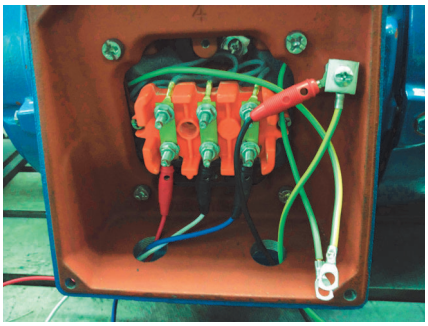

(e) Shield connections (two unconnected lines) routed to the terminal box.

Fig. 8: Preparation and installation of aluminium foil end-winding shields.

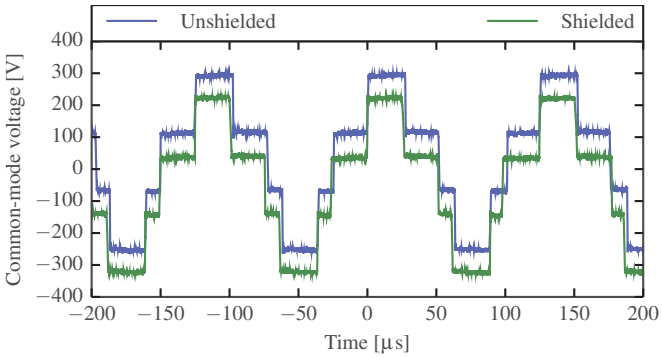

(a) Common-mode voltage.

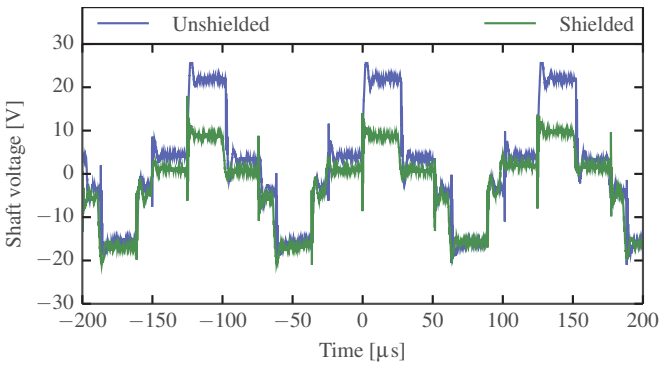

(b) Shaft voltage.

Fig. 9: Comparison of common-mode and shaft voltages with unshielded and shielded end-winding regions.

TABLE III: Comparison of shielding configurations

Shields	**Common-mode voltage**	**Shaft voltage**	**Full-load efficiency**
None	545 V	37 V	88.8 %
End-winding	545 V	25 V	88.8 %
Full	545 V	0.4 V	87.5 %

waveforms for the unshielded and shielded configurations are presented in Fig. 11. In this case, it can be seen that the shields almost completely eliminate the shaft voltage.

Because having additional conductive material installed in the air-gap of the machine can lead to additional eddy current losses, simple full-load efficiency tests were conducted with and without these shields installed. It was found that the fully shielded configuration did have a slightly lower efficiency, indicating that some losses were generated in the shields.

A summary of the results is presented in Table III.

V. Conclusions and Future Work

This paper has described different inverter-induced bearing current phenomenon. Among these, *electrostatic discharge machining* (EDM) bearing currents are the most troublesome in low voltage induction machines. Electrostatic shielding has been identified as a promising solution to EDM bearing currents. Although partial shields covering only the end-windings have resulted in a significant reduction in the shaft voltage, it is likely that these shields will not eliminate the problem since shaft voltages in the range of 20 V were

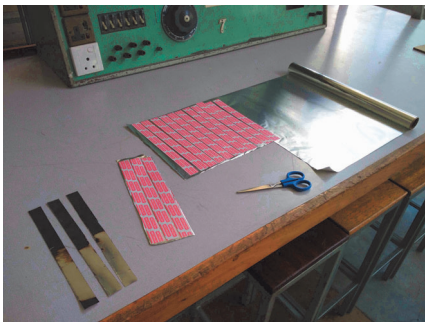

(a) Fabrication of shielding strips.

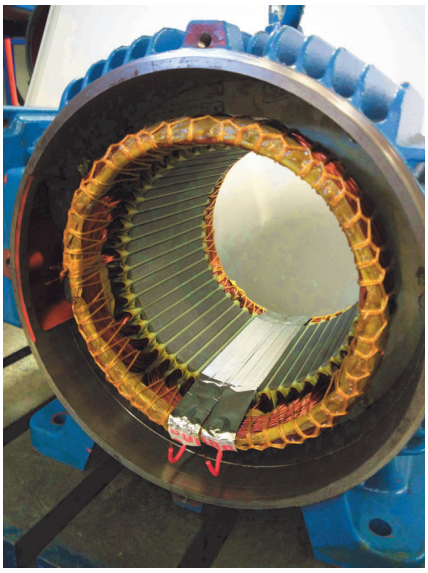

(b) Installation of shielding strips.

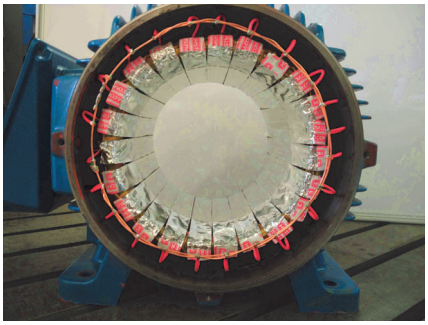

(c) Shielding installed and connected to ground ring.

Fig. 10: Preparation and installation of full air-gap shields.

still observed. Thus, it can be concluded that more elaborate shields are required in order to completely eliminate EDM bearing currents.

It has been demonstrated that a fully shielded configuration, enclosing the end-windings and the inner bore of the stator can almost completely eliminate the shaft voltage. However, shielding in the air-gap or slot regions cause additional eddy current losses which will need to be kept to a minimum in order for the method to be acceptable.

Complete shielding of the winding inside the stator slots is another alternative that can be considered in future work. This configuration may also be able prevent high frequency

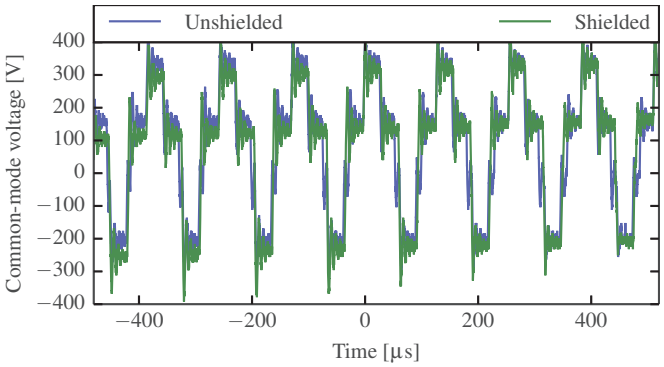

(a) Common-mode voltage.

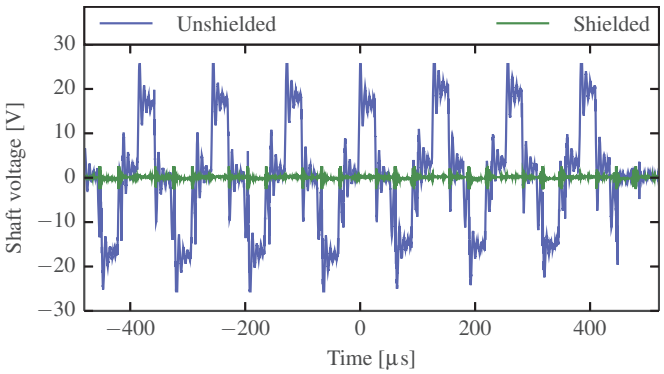

(b) Shaft voltage.

Fig. 11: Comparison of common-mode and shaft voltages with unshielded and fully shielded rotor.

circulating bearing currents. Modifications to the winding insulation system that incorporate an effective, low-loss shielding material may be an effective way to implement such shields.

Acknowledgment

This work was supported by ABB Corporate Research, Sweden.

References

[1] I. Kerszenbaum, "Shaft currents in electric machines fed by solid-state drives," in *IEEE Industrial and Commercial Power Systems Technical Conference*, May 1992, pp. 71–79.

[2] S. Chen, T. A. Lipo, and D. Fitzgerald, "Source of induction motor bearing currents caused by PWM inverters," *IEEE Transactions on Energy Conversion*, vol. 11, no. 1, pp. 25–32, Mar. 1996.

[3] S. Chen, T. A. Lipo, and D. W. Novotny, "Circulating type motor bearing current in inverter drives," in *IEEE Industry Applications Conference, IAS Annual Meeting*, vol. 1, Oct. 1996, pp. 162–167.

[4] A. Muetze, "On a New Type of Inverter-Induced Bearing Current in Large Drives with Oil-Lubricated Bearings," in *IEEE Industry Applications Society Annual Meeting*, Oct. 2008, pp. 1–8.

[5] P. Maki-Ontto, "Modeling and Reduction of Shaft Voltages in AC Motors fed by Frequency Converters," Ph.D. dissertation, Helsinki University of Technology, 2006.

[6] R. F. Schiferl, M. J. Melfi, and J. S. Wang, "Inverter driven induction motor bearing current solutions," in *IAS Petroleum and Chemical Industry Conference*, 2002, pp. 67–75.

[7] D. Busse, J. Erdman, R. J. Kerkman, D. Schlegel, and G. Skibinski, "System electrical parameters and their effects on bearing currents," *IEEE Transactions on Industry Applications*, vol. 33, no. 2, pp. 577–584, Mar. 1997.

[8] P. Maki-Ontto and J. Luomi, "Induction motor model for the analysis of capacitive and induced shaft voltages," in *IEEE International Conference on Electric Machines and Drives*, May 2005, pp. 1653–1660.

[9] A. Muetze and A. Binder, "Calculation of Motor Capacitances for Prediction of the Voltage Across the Bearings in Machines of Inverter-Based Drive Systems," *IEEE Transactions on Industry Applications*, vol. 43, no. 3, pp. 665–672, May 2007.

[10] O. Magdun, Y. Gemeinder, and A. Binder, "Prevention of harmful EDM currents in inverter-fed AC machines by use of electrostatic shields in the stator winding overhang," in *36th Annual Conference on IEEE Industrial Electronics Society*, Nov. 2010, pp. 962–967.

[11] O. Magdun and A. Binder, "Calculation of roller and ball bearing capacitances and prediction of EDM currents," in *35th Annual Conference of IEEE Industrial Electronics*, Nov. 2009, pp. 1051–1056.

[12] D. F. Busse, J. M. Erdman, R. J. Kerkman, D. W. Schlegel, and G. L. Skibinski, "An evaluation of the electrostatic shielded induction motor: a solution for rotor shaft voltage buildup and bearing current," *IEEE Transactions on Industry Applications*, vol. 33, no. 6, pp. 1563–1570, Nov. 1997.

[13] F. J. T. E. Ferreira, M. V. Cistelecan, and A. T. d. Almeida, "Evaluation of Slot-Embedded Partial Electrostatic Shield for High-Frequency Bearing Current Mitigation in Inverter-Fed Induction Motors," *IEEE Transactions on Energy Conversion*, vol. 27, no. 2, pp. 382–390, Jun. 2012.